Microsc. Microanal. 12, 285–294, 2006
DOI: 10.1017/S1431927606060363

Microscopy AND Microanalysis

© MICROSCOPY SOCIETY OF AMERICA 2006

Quantitative Strain Mapping Applied to Aberration-Corrected HAADF Images

Ana M. Sanchez,[1,*] Pedro L. Galindo,[2] Slawomir Kret,[3] Meiken Falke,[4] Richard Beanland,[5] and Peter J. Goodhew[6]

[1]*Departamento de Ciencia de los Materiales e I. M. y Q.I., Universidad de Cadiz, Puerto Real 11510, Spain*
[2]*Departamento de Lenguajes y Sistemas Informaticos, Universidad de Cadiz, Puerto Real 11510, Spain*
[3]*Institute of Physics, Polish Academy of Science, Al. Lotnikow 32/46. PL-020668 Warzawa, Poland*
[4]*UK SuperSTEM, Daresbury Laboratory, Daresbury WA4 4AD, United Kingdom*
[5]*Bookham Technology, Caswell, Towcester, Northants NN12 8EQ, United Kingdom*
[6]*Department of Engineering, University of Liverpool, Liverpool L69 3GH, United Kingdom*

Abstract: A systematic distortion in high-angle annular dark-field scanning transmission electron microscope (HAADF-STEM) images, which may be caused by residual electrical interference, has been evaluated. Strain mapping, using the geometric phase methodology, has been applied to images acquired in an aberration-corrected STEM. This allows this distortion to be removed and so quantitative analysis of HAADF-STEM images was enabled. The distortion is quantified by applying this technique to structurally perfect and strain-free material. As an example, the correction is used to analyse an InAs/GaAs dot-in-quantum well heterostructure grown by molecular beam epitaxy. The result is a quantitative measure of internal strain on an atomic scale. The measured internal strain field of the heterostructure can be interpreted as being due to variations of indium concentration in the quantum dot.

Key words: HAADF, STEM, distortion, nanostructures, algorithm, strain, InAs

Introduction

Materials science depends on relating microscopic structure to macroscopic behavior. As fabrication methods approach the atomic scale, new techniques must be developed capable of characterizing a sample of only a few thousand atoms. One of the main engines of this drive to smaller length scales is the microelectronics industry, which already employs devices that are a few tens of nanometers in size in production processes. Developing analysis techniques that are capable of matching this technology is one of the major challenges in materials science.

The development of high-resolution transmission electron microscopy (HRTEM), such as quantitative HRTEM (Bierwolf et al., 1993; Kret et al., 2001), scanning TEM (STEM), and similar techniques allows imaging of most crystalline materials, supplying information on the structure of defects at the atomic level and also chemical composition at subnanometer levels. In the past few years, considerable advances have been achieved in quantitative analysis at a very high spatial resolution, based on conventional HRTEM images (Rosenauer et al., 1997; Hÿtch & Plamann, 2001; Kret et al., 2001). Data related to displacement and strain fields may be analyzed using different techniques for strain mapping, such as geometric phase (Hÿtch et al., 1998) or peak pairs (Galindo et al., 2006). Nevertheless, any technique based on HRTEM is sensitive to variations in sample thickness and changes in focus conditions, which can make quantitative analysis a complex task. HRTEM images are much more sensitive to local variations in sample thickness and changes in focus conditions in comparison with high-angle annular dark-field scanning transmission electron microscopy (HAADF-STEM) images. Thus it may be possible to apply strain mapping techniques using HAADF-STEM to samples that could not be tackled by HRTEM. For both techniques, specimen drift can cause problems. For HRTEM, drift produces a degradation of the whole image, whereas for STEM images, it appears as an image distortion. Thus caution is required in analyzing strains in HAADF-STEM images, particularly because acquisition times are usually much longer.

The spherical aberration coefficient, C_s, of the objective lens is one of the main parameters that limits TEM resolution. For dedicated STEM microscopes, correction of the spherical aberration of the objective lens using a set of quadrupole and octupole lenses has recently become available (Krivanek et al., 1999). This allows the formation of a sub-Ångstrom probe for ultra-high-resolution high-angle

Received August 18, 2005; accepted March 29, 2006.
*Corresponding author. E-mail: ana.fuentes@uca.es

annular dark-field (HAADF) imaging. Conventional HRTEM images of sufficient quality for quantitative analysis can only be obtained from very thin samples (5–20 nm thickness). On the other hand, STEM-HAADF gives high-resolution images from somewhat thicker areas of the sample, which can be a great advantage. The HAADF signal is strongly related to the atomic number Z of the scattering atoms; therefore its combination with strain measurement is a powerful tool for analysis in crystalline semiconductor materials, because it gives a two-pronged approach.

In this article we present an application of geometric phase methodology to the aberration-corrected HAADF-STEM images of an InAs/GaAs dot-in-well heterostructure using strain mapping techniques. Strain mapping of unstrained GaAs using geometric phase was also used to measure systematic distortions in HAADF images. In this article we apply the algorithm developed in Sanchez et al. (2006). We can correct the HAADF images using the systematic distortion measurement in undistorted parts of the sample. Subsequently, geometric phase and analysis is applied to the corrected HAADF-STEM images of an InAs/GaAs dot-in-well structure. Strain measurements, which are related to the compositional changes in the heterostructure, have been obtained in different areas containing quantum dots. We are therefore able to show that a quantitative HRTEM methodology can be applied to HAADF images from an aberration-corrected dedicated STEM.

Materials and Methods

The sample was an InAs quantum dots-in-well (DWELL) structure grown in a VG V100 MBE system. Initially a 200-nm GaAs buffer was grown, followed by a 100 nm AlGaAs PL cladding layer and then 150 nm of GaAs, all at 600°C. For dot growth, the temperature was reduced to 510°C and a 2-nm $In_{0.15}Ga_{0.85}As$ layer was grown, followed by 0.8 nm of InAs, deposited at 0.025 ml/s. The dots were capped with 6 nm of $In_{0.15}Ga_{0.85}As$ followed by a 15-nm GaAs layer. The substrate temperature was then increased back to 600°C and a further 35 nm of GaAs deposited. This process was repeated three times and the whole structure was capped with 100 nm GaAs followed by a 100-nm AlGaAs cladding layer, capped with 10 nm GaAs.

Cross-sectional TEM specimens were prepared in the usual manner (Beanland, 2003), that is, by mechanical grinding to below 20 μm and mechanical polishing using 1 μm diamond suspension on a soft nap pad. The specimens were ion milled to electron transparency using Ar^+ ions at 6 kV and a beam incidence angle of 3° (uncooled). A final low-energy cleansing of the sample at 2 kV was employed to minimize amorphous surface layers. Conventional TEM was carried out on a JEOL 100CX microscope operating at 120 kV, close to the $[110]_{GaAs}$ zone axis. Further investigations were carried out using a VG HB501 UX FEG-STEM equipped with the recently developed Nion spherical aberration corrector operating at 100 kV (SuperSTEM).

All STEM images were recorded under the same conditions, with 50-Hz line synchronization, with the x-axis parallel to the scan lines. A large fly back time was chosen to reduce the influence of small beam deflections and hysteresis effects on the HAADF images. HAADF images were recorded from several areas corresponding to the GaAs substrate at different magnifications and scan times to determine and remove the systematic distortion in the images. Additionally, HAADF images in areas containing InAs quantum dots were obtained to analyze the strain distribution in the InAs dot-in-well heterostructure.

Our processing started with a noise reduction procedure with the use of a combination of the Wiener filter in Fourier space. The noise estimator necessary for the Wiener filter was obtained by interpolation of the background on the power spectrum image. To avoid the contribution of the strong Bragg peaks, an interpolation procedure similar to that proposed by Rosenauer was applied (Rosenauer et al., 1997). For 1024×1024 pixel images, the estimation of the noise distribution in the Fourier space was made with blocks of 16×16 pixels. Additionally the Bragg filter generated with circular "holes" having a diameter of 50 pixels, smoothed to gradually decrease from 99% to 1% in 6 pixels, centered at the positions of the Bragg spots of the periodic part of the image, which in this case is three symmetric spots corresponding to the cubic structure of InAs. Due to the big size of the mask as well during the Wiener filtering procedure, the information about distortion that is usually located near the Bragg peak was conserved. This noise reduction was successfully applied for measurement of strain from HRTEM images and reduced mainly a random shift of the fringes fluctuation coming from the amorphous layer.

The geometric phase algorithm calculates the displacement field from the phase images for two different and noncollinear vectors. Gaussian masks were placed around two different (111) peaks in the power spectrum in this case. The phase image is approximately zero in the reference area, as this corresponds to the area of the crystal chosen as the reference lattice. To further refine the vector **g**, a small area in the uniform unwrapped phase image was chosen, typically far away from the stressed area, and its averaged lattice spacing was calculated. The displacement field is given by solving these simultaneous equations:

$$\begin{pmatrix} P_{g1} \\ P_{g2} \end{pmatrix} = -2\pi \begin{pmatrix} g_{1x} & g_{1y} \\ g_{2x} & g_{2y}y \end{pmatrix} \begin{pmatrix} u_x \\ u_y \end{pmatrix}$$

where P_g is the phase image, g_x and g_y the k_x and k_y components of the vector **g** and u_x and u_y are the x and y components of the displacement field at position $r = (x, y)$. Next the systematic lattice distortion tensors β_{ij}, defined as

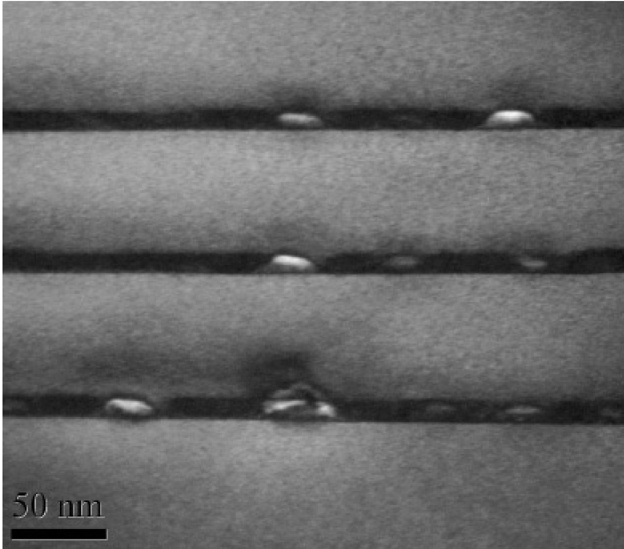

Figure 1. Dark field 002 TEM image, showing the InAs/GaAs quantum dot heterostructure. The InAs dots appear with a bright contrast inside an InGaAs quantum well (dark contrast). GaAs barriers between each DWELL structure show a mid-gray contrast.

the variation of the displacements in the i direction with respect to j (i.e., $\beta_{yx} = \partial u_y/\partial x$) were calculated (Hÿtch & Plamann, 2001; Kret et al., 2001).

Once these measures have been obtained, these can be used to produce an image in which pixels have intensities corresponding to the intensity in the original image after the systematic distortion is removed (Sanchez et al., 2006).

Results and Discussion

A dark-field 002 TEM image of the structure is shown in Figure 1. Because this reflection is sensitive to material composition (Bithell & Stobbs, 1989, 1991), bright regions correspond to the InAs quantum dots inside dark layers of $In_xGa_{1-x}As$, surrounded by mid-gray GaAs material. The dot size is quite large, 15–25 nm wide and 7–10 nm high.

Figure 2 shows a HAADF image of the GaAs substrate with the beam parallel to the [110] axis, with an image size of 1024 × 1024 pixels and magnification of 0.04170 nm/pixel (indicated magnification 500,000×). A bending of the (002) and (111) lattice planes is readily observed in these images, even though the material is the unstrained GaAs substrate. A band pattern was observed in the u_y displacement component (Sanchez et al., 2006), which is due to the slight movement of the beam during each scanned line, possibly (but not necessarily) due to 50-Hz electrical noise. The vertical band patterns observed in u_y (not shown in this article) are also visible in the maps of the derivative of the displacement β_{yx} (Fig. 3d) and with a much lower amplitude in β_{xx} (Fig. 2a), but they are not apparent in the other strain maps (β_{yy}, β_{xy}) (Fig. 3b,c). In Figure 4, the mean profiles obtained by column averaging and the mean plus/minus one standard deviation profiles on each column across the different strain maps are plotted. The standard deviation of the pixel values in β_{yx} was equal to 0.0186, whereas other strain maps ($\beta_{xx}\beta_{yy}, \beta_{xy}$) have pixel standard deviations equal to 0.0094, 0.0115, and 0.0105, respectively. An exhaustive analysis of the systematic distortion with

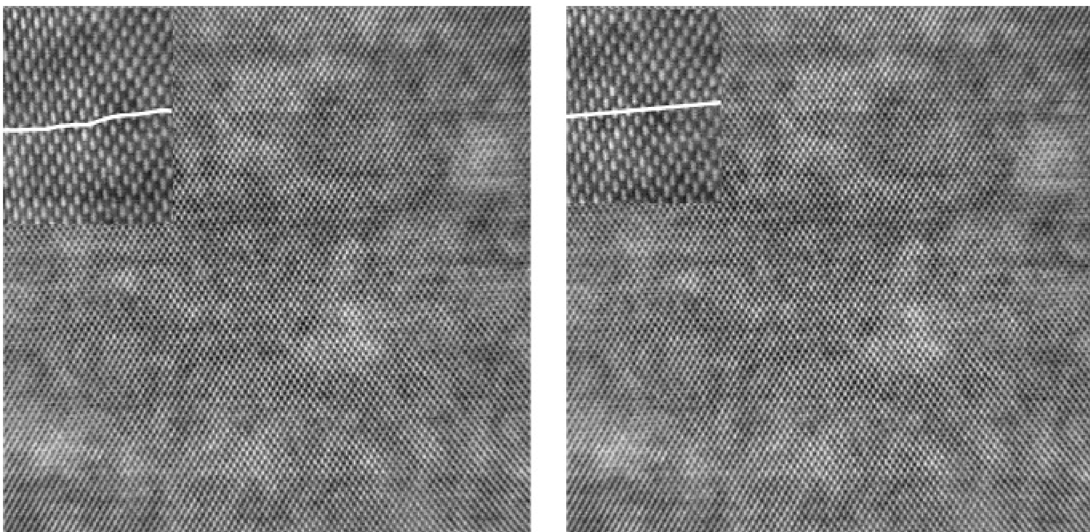

Figure 2. **a:** HAADF image of strain-free GaAs recorded at 500,000×. **b:** Distortion-corrected image of the same image, after applying the correction procedure. A magnified image is inset in the left top corner of each image, demonstrating the correction of bending planes.

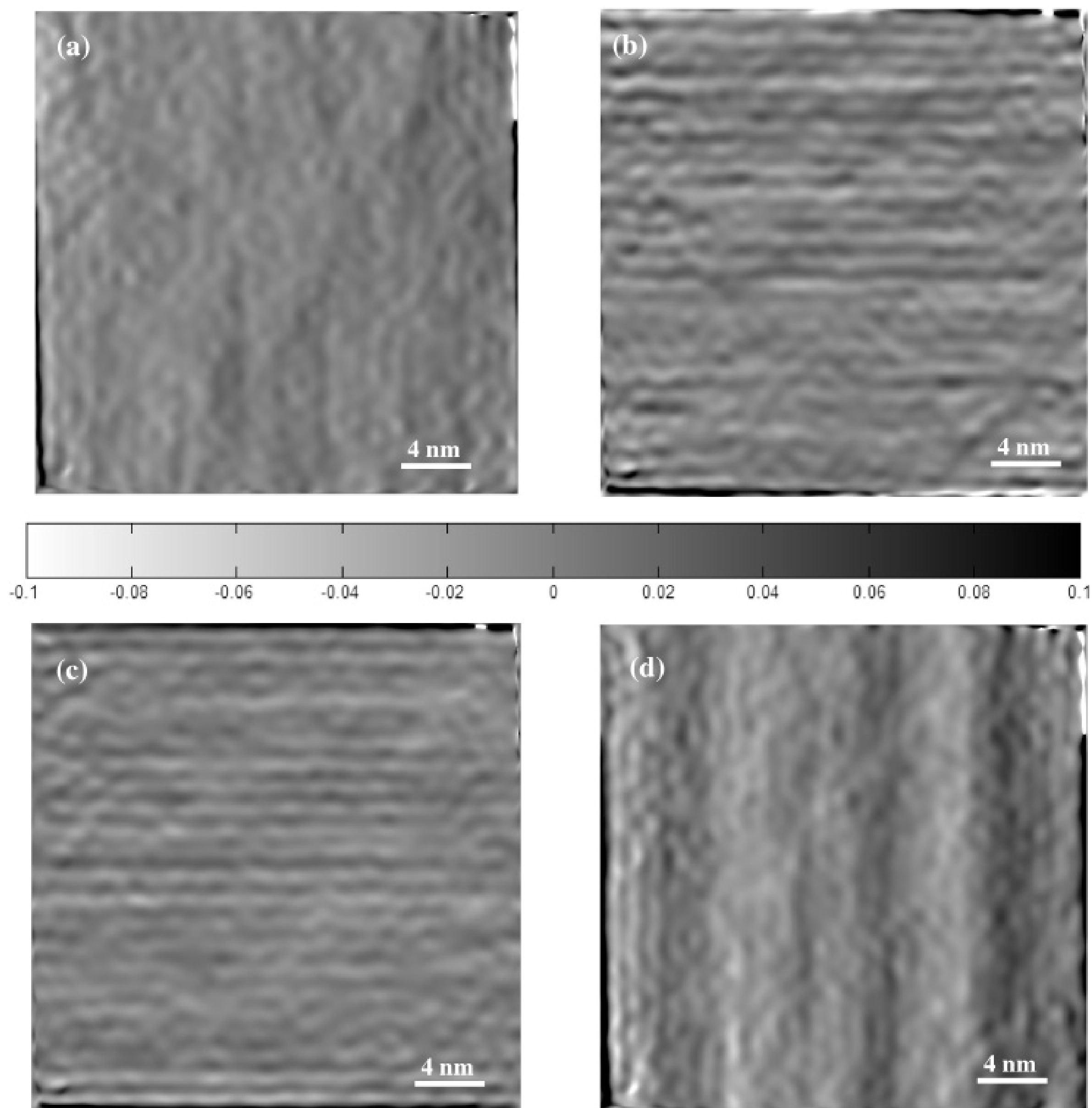

Figure 3. β_{xx} (**a**), β_{yy} (**b**), β_{xy} (**c**), and β_{yx} (**d**) components of the distortion tensor before applying the correction procedure. Note the banded pattern in the β_{yx} component.

time and magnification, considering all its components, can be found in Sanchez et al. (2006). The systematic distortion was found to be essentially the same for different images obtained at the same magnification, although the β_{yx} distortion component varied in proportion with the magnification. This fact clearly confirms that distortion in the GaAs unstrained region is due to the scanning process and not the result of low-frequency sample vibration or drift.

The main result of the strain mapping analysis was that the y component of the displacement changes with the x coordinate produces considerable "waves" in the image. On the other hand, the x component of the displacement was not strongly affected by the systematic distortion. This allows us to conclude that the main distortion is a shift of the columns of pixels in the y direction. The HAADF images were corrected following the methodology and algorithm developed by Sanchez et al. (2006). Figure 2b shows the recalculated image, correcting for these distortions. The bending of the lattice planes is not observed. A clearer demonstration of the systematic deformation removal is shown in Figures 5 and 6, where the β_{yx} distortion tensor component does not show the vertical stripes seen in the original image, and the amplitude of the β_{yx} distortion component after the correction was reduced considerably.

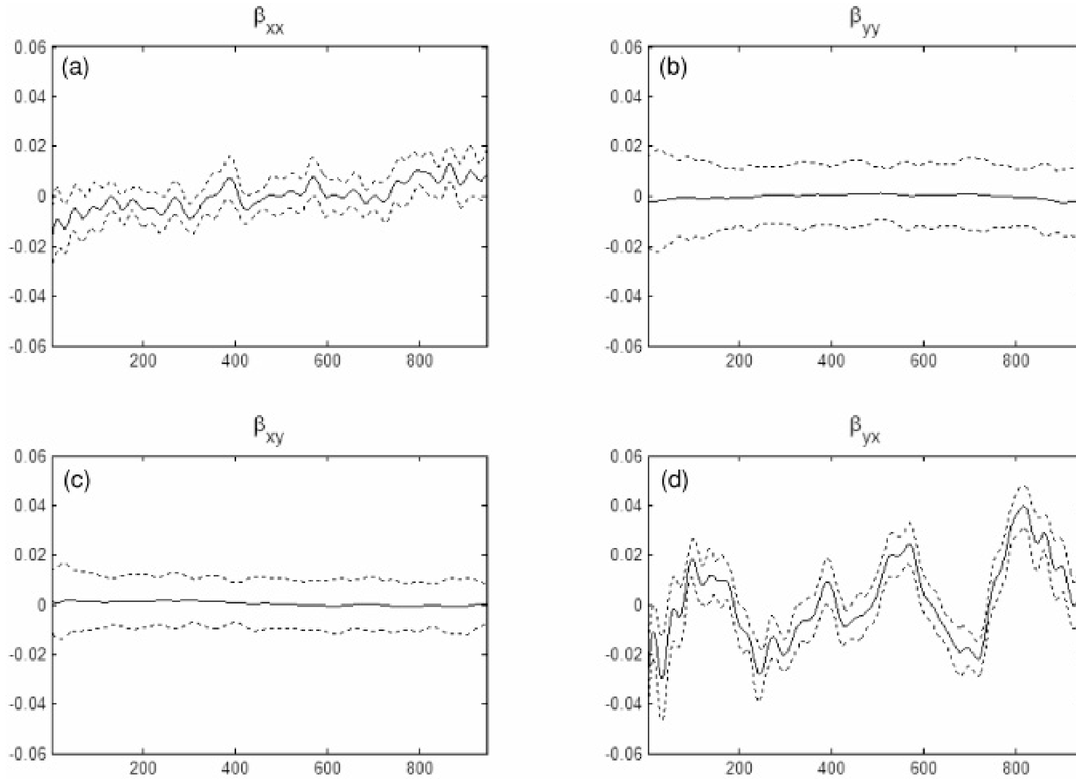

Figure 4. β_{xx} (**a**), β_{yy} (**b**), β_{xy} (**c**), and β_{yx} (**d**) mean profiles before applying the correction procedure. Mean and mean plus and minus standard deviations are plotted.

The unit cells of the strained material in epitaxial layers are tetragonally distorted; that is, the lattice parameter parallel to the interface plane adopts the parameter of the substrate, and the parameter perpendicular to the interface varies following the Poisson effect. The systematic distortion in the HAADF images is not critical in tetragonal distortion measurements, because the periodicity is correct in β_{yy} as can be observed in Figures 3b and 5b. The amplitude of the mean distortion was very small and the pixel standard deviation was reduced to 0.0095, 0.0116, 0.0105, and 0.0101 for β_{xx}, β_{yy}, β_{xy}, and β_{yx}, respectively. The columns of pixels are slightly shifted in the y direction, but the periodicity of crystal is preserved. However, any other measurement will be affected by the distortion, and so we have used this approach to produce distortion-corrected images.

We now present an example of strain determination in a DWELL structure. The HAADF images were recorded with the growth direction parallel to the y scan. The measured distortions in areas corresponding to relaxed GaAs substrate were used to correct the original images and remove the systematic distortion. Figure 7 shows the comparison between the strain analysis carried out in the HAADF image containing the quantum dot before and after the correction procedure. Figure 7a is a typical HAADF image that has been used for the evaluation of the strain. An InAs quantum dot can be observed in the center of this image. The strain distribution in the HAADF image (Fig. 7a) is shown in Figure 7b. Applying the algorithm allowed us to produce an image without systematic deformation (Fig. 7c). Following the same methodology as described above, the strain distribution was obtained in this new calculated image (Fig. 7d). Because the y periodicity is correct, as noted above, no significant differences are present between Figures 7b and 7d. The main limitation of the strain measurement applied to the STEM image is the random horizontal strips, which cannot be corrected with our procedure. These can be strongly reduced by averaging strained maps from different exposures. If the observed sample does not change significantly under the electron beam, the error of the strain mapping of HAADF images can be similar to that obtained from HRTEM images (i.e., 0.2% with 1 nm spatial averaging; Kret et al., 2001).

From the full set of analyses we can conclude that the strain map clearly shows maxima in areas corresponding to the InAs, which can be attributed to the highest concentration of In in those areas. The misfit between GaAs and InAs is 7.2%. However, the measured strain (in relation to GaAs) in the InAs has a maximum value around 10%—this larger value is to be expected, due to the Poisson effect. We can clearly differentiate the areas corresponding to the quantum

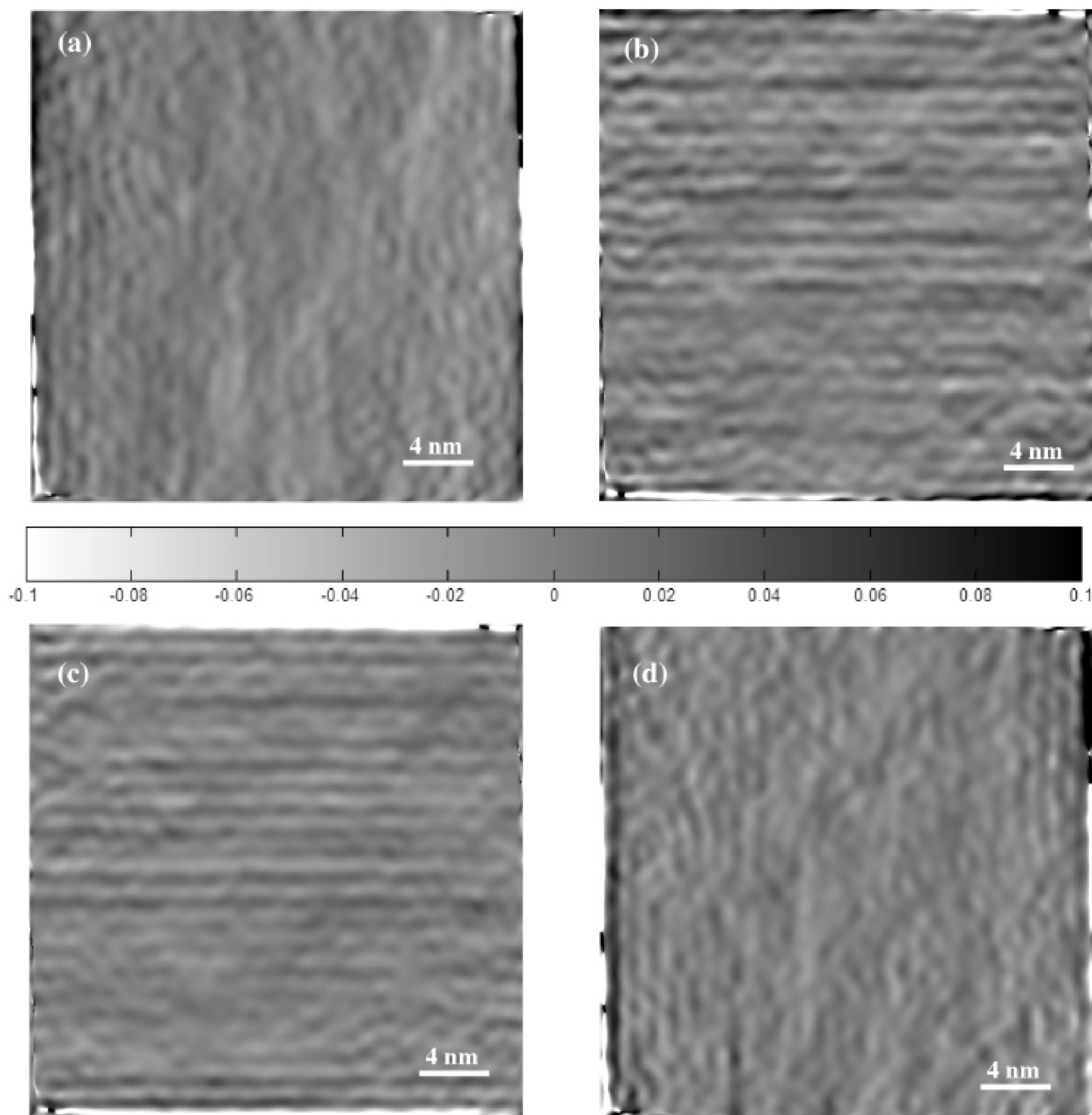

Figure 5. β_{xx} (**a**), β_{yy} (**b**), β_{xy} (**c**), and β_{yx} (**d**) components of the distortion tensor after applying the correction procedure. No banded pattern is present in the β_{yx} component, thus preserving the periodicity of the crystal in the y direction.

dot, which seems to be nonhomogeneous in In composition. This procedure has been repeated in different areas around the quantum dot as shown in Figure 8. In Figure 8a part of a quantum dot is to the right center of the image, and in Figure 8c, the quantum dot can be observed in the upper part of the image. The strain distribution obtained for these images is shown in Figures 8b and 8d, respectively. From this set of analysis we can conclude that the strain distribution in the InAs/GaAs heterostructure can be obtained as shown in Figures 7 and 8. The relatively large areas of highest strain correspond to the areas containing the quantum dot. The quantum well region is less visible; this may be because the strain in the well is relatively low in comparison with that in the dot; also the field of view is not sufficiently large to be able to assign a well-defined region of the image to the well. Some small regions are also present with very high strain values ($>$10%). As these are reproduced in the different images, they are clearly a real effect in the sample. However as there are no longer-range strain fields associated with them, they are unlikely to be crystal defects; they are most likely artifacts associated with sample preparation (e.g., an amorphous surface layer).

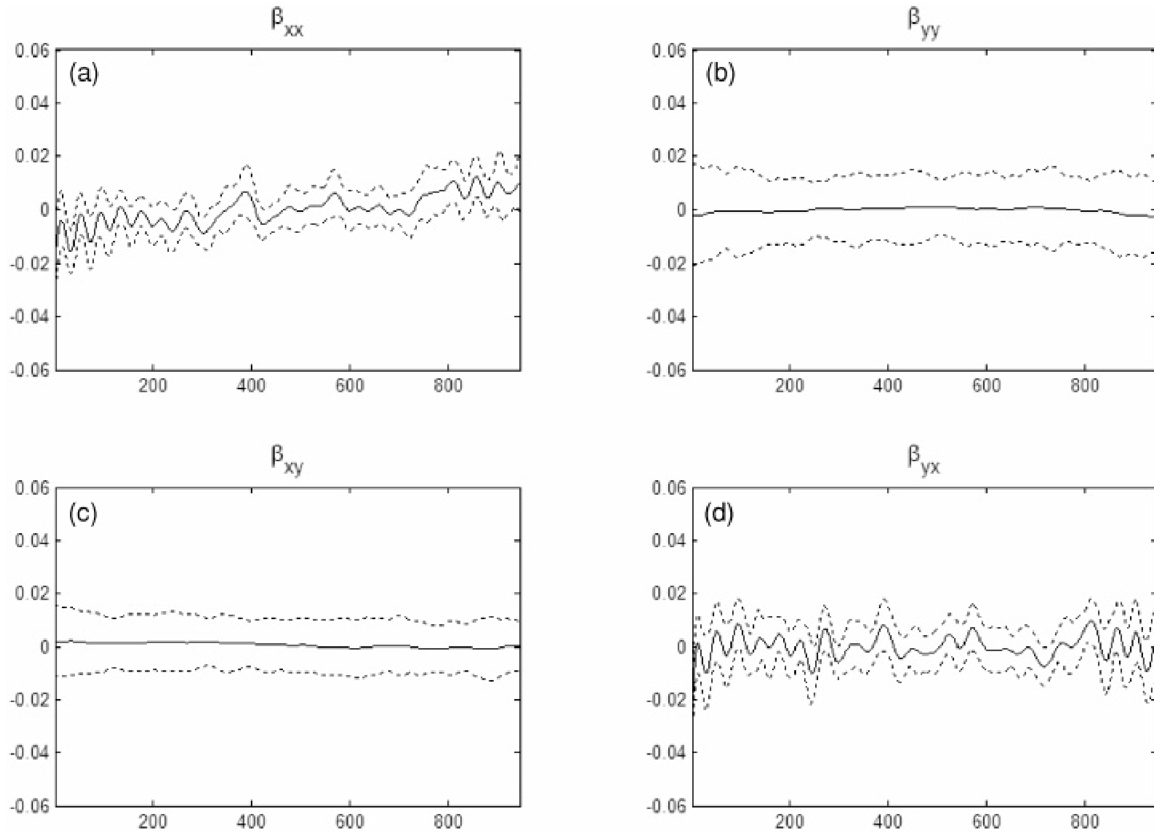

Figure 6. β_{xx} (**a**), β_{yy} (**b**), β_{xy} (**c**), and β_{yx} (**d**) mean profiles after applying the correction procedure. Mean and mean plus and minus standard deviation are plotted. The β_{yx} mean component has been reduced to the same level as others.

At this point we should consider the relaxation of the tetragonally distorted lattice due to the presence of the free surfaces of the TEM specimen. The relationship between lattice spacings perpendicular and parallel to the growth direction is (Rosenauer, 2003)

$$\frac{a_s - a_\perp}{a_s} = A\,\frac{a_s - a}{a_s}, \quad (1)$$

where a_s is the substrate parameter (GaAs), a is the dot lattice parameter (InAs), and $a_\perp$ the lattice parameter perpendicular to the interface. The value of A depends on the elastic constant of the strained layer. For a cubic crystal with the electron beam along a $\langle 110\rangle$ direction A is given by

$$A_{\text{thick}} = \left(1 + 2\,\frac{C_{12}}{C_{11}}\right) \quad (2a)$$

$$A_{\text{thin}} = \left(1 + 4\,\frac{C_{44}C_{12}}{C_{11}^2 + 2C_{11}C_{44} + C_{11}C_{12} - 2C_{12}^2}\right), \quad (2b)$$

where A_{thick} and A_{thin} refer to a very thick (essentially bulk) and a very thin (essentially relaxed) specimen. Using equations (2), for an experimental strain of 10%, the concentration of In lies between 90% and 66%, depending whether we consider the sample as a thin foil or as bulk material. This is a large range, and it illustrates the difficulty of obtaining accurate results based on strain analysis of thin TEM sections by any technique. In similar HRTEM studies of an InGaN/GaN quantum well heterostructure, the uncertainty in composition was reduced by modeling the real sample geometry (Ruterana et al., 2002). The use of finite element simulations could provide a better determination of the In concentration.

Conclusions

We have demonstrated that strain mapping is a powerful tool for analyzing HAADF images. The systematic distortion in the HAADF images was found to be essentially constant with time. This makes it possible to produce

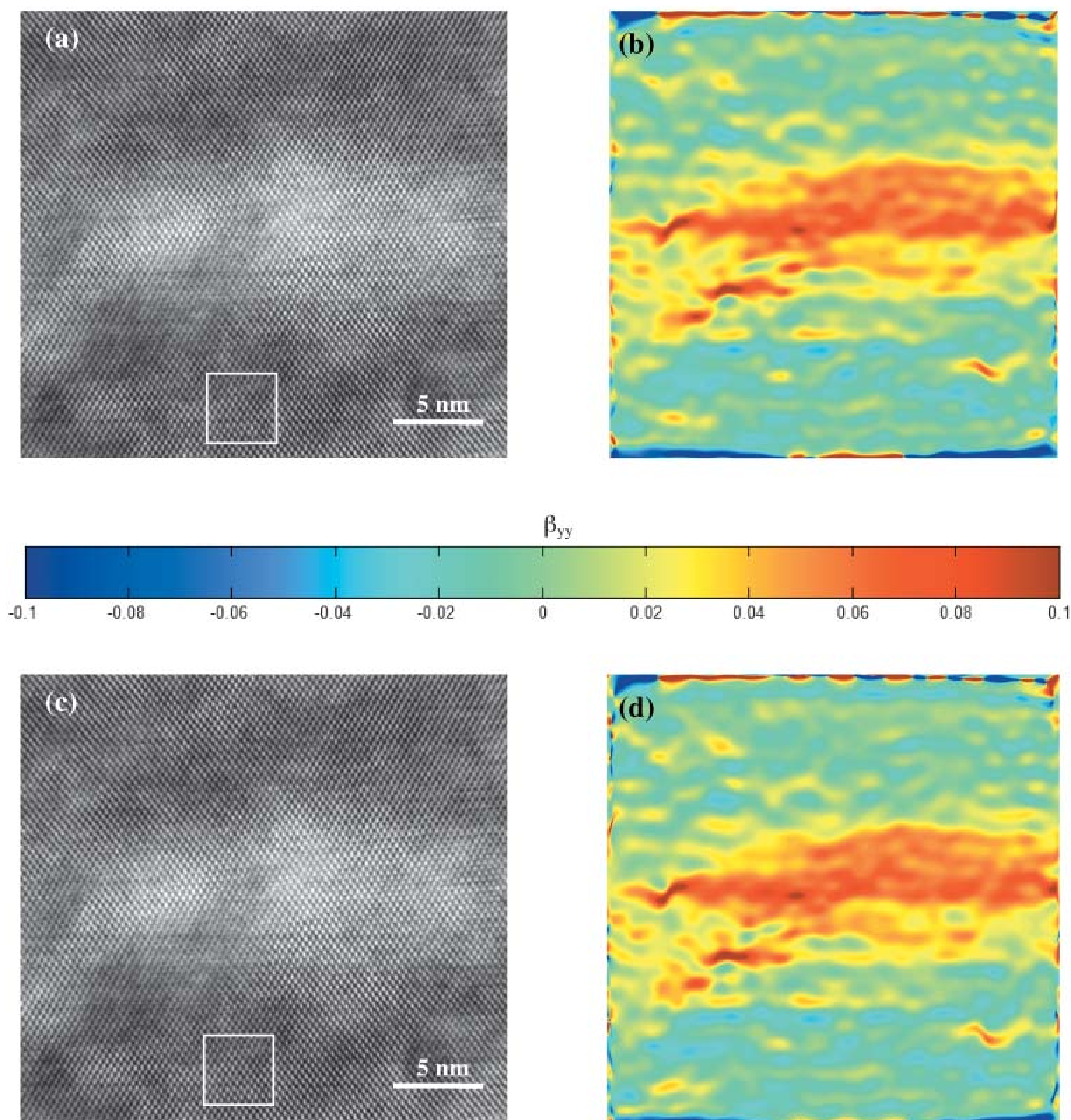

Figure 7. a: HAADF image of InAs/GaAs quantum dots along the ⟨110⟩ zone axis. A quantum dot is in the center of the image; growth direction isvertically upward. **b:** β_{yy} strain field distribution, where the maxima strain can be attributed to the presence of indium in the quantum dot. **c:** Calculated HAADF images of the InAs/GaAs quantum dot where the systematic distortion has been removed. **d:** Strain field distribution corresponding to image **c**. The white square in **a** and **c** indicates the chosen reference area in the uniform unwrapped phase images.

distortion-free images of material that contains internal strain fields and, using the same tools that are used to characterize the systematic distortion, a quantitative analysis of internal strain can be performed. Thus STEM microscopy has the potential to perform quantitative analyses with HAADF images in the same way as can be done with conventional HRTEM images, with the potential to use thicker regions of the sample. More work is needed to link the internal strain and the compositional variations within the sample. Finite element analysis is one route; it may also be possible to use the atomic number contrast also present in HAADF images.

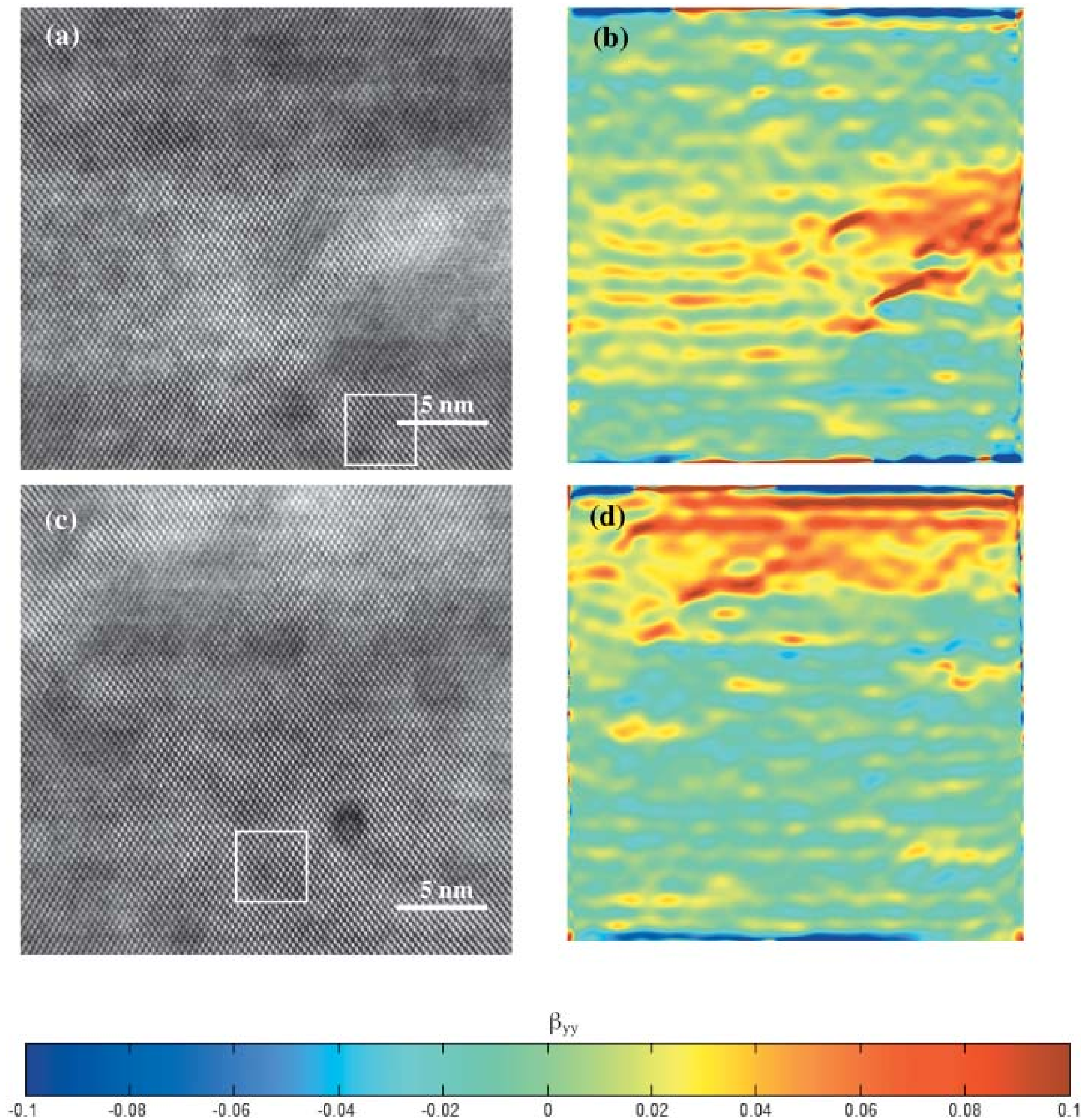

Figure 8. **a:** HAADF image of InAs/GaAs quantum dots along the ⟨110⟩ zone axis. A quantum dot is in the center right of the image; growth direction is vertically upward. **b:** Strain field distribution corresponding to **a**. **c:** An image similar to **a** with a quantum dot to the top of the image. **d:** Strain field distribution corresponding to **c**. The white square in **a** and **c** indicates the chosen reference area in the uniform unwrapped phase images.

Acknowledgments

The authors acknowledge financial support from EPSRC and SANDIE European Network of Excellence (NNPA-CT-2004-500101 Sixth Framework Program) for many aspects of this work.

References

Beanland, R. (2003). Rapid cross-section TEM specimen preparation of III-V materials. *Microsc Today* **11**, 29–31.

Bierwolf, R., Hohenstein, M., Phillipp, F., Brandt, O., Crook, G.E. & Ploog, K. (1993). Direct measurement of local lattice-distortions in strained layer structures by HREM. *Ultramicroscopy* **49**, 273–285.

Bithell, E.G. & Stobbs, W.M. (1989). Composition determination in the GaAs/(Al, Ga)As system using contrast in dark-field transmission electron-microscope images. *Philos Mag A* **60**, 39–62.

Bithell, E.G. & Stobbs, W.M. (1991). III-V ternary semiconductor heterostructures—The choice of an appropriate compositional analysis technique. *J Appl Phys* **69**, 2149–2155.

Galindo, P.L., Yañez, A., Pizarro, J., Guerrero, E., Ben, T. & Molina, S.I. (2006). Strain mapping from HRTEM images. In

Proceedings of the Microscopy of Semiconducting Materials XIV Conference. Oxford: Institute of Physics (in press).

Hÿtch, M.J. & Plamann, T. (2001). Imaging conditions for reliable measurement of displacement and strain in high-resolution electron microscopy. *Ultramicroscopy* **87**, 199–212.

Hÿtch, M.J., Snoeck, E. & Kilaas, R. (1998). Quantitative measurement of displacement and strain fields from HREM micrographs. *Ultramicroscopy* **74**, 131–146.

Kret, S., Ruterana, P., Rosenauer, A. & Gerthsen, D. (2001). Extracting quantitative information from high resolution electron microscopy. *Phys Stat Sol B* **227**, 247–295.

Krivanek, O.L., Dellby, N. & Lupini, A.R. (1999). Towards subangstrom electron beams. *Ultramicroscopy* **78**, 1–11.

Rosenauer, A. (2003). *Transmission Electron Microscopy of Semiconductor Nanostructures. An Analysis of Composition and Strain State*. Berlin: Springer.

Rosenauer, A., Remmele, T., Gerthsen, D., Tillmann, K. & Förster, A. (1997). Atomic scale strain measurements by the digital analysis of transmission electron microscopic lattice images. *Optik* **105**, 99–107.

Ruterana, R., Kret, S., Maciejewski, G. & Dluzewski, P. (2002). Composition fluctuation in InGaN quantum wells made from molecular beam or metalorganic vapor phase epitaxial layers. *J Appl Phys* **91**, 8979–8985.

Sanchez, A.M., Galindo, P.L., Kret, S., Falke, M., Beanland, R. & Goodhew, P.J. (2006). An approach to the systematic distortion correction in aberration corrected HAADF images. *J Microsc* **221**, 1–7.